

Supplementary Information for  
“Crack formation and self-closing  
in shrinkable, granular packings”

H. Jeremy Cho, Nancy B. Lu, Michael P. Howard,  
Rebekah A. Adams, and Sujit S. Datta

# Supplementary Discussion

## The perfect-crystal model in comparison to the Griffith model of cracking

In our model, we assume a perfect crystal; thus, the criterion for RC fracture is simply when the stress is equivalent to the capillary stress:

$$\sigma_{\text{cap}} \sim \frac{\gamma}{R}. \quad (1)$$

In the Griffith criterion of stress, however,

$$\sigma_{\text{Griffith}} \sim \sqrt{\frac{\gamma \mathcal{E}}{R_{\text{wet}}}}. \quad (2)$$

where we assume the defect length is on the order of  $R_{\text{wet}}$ . If we substitute our effective modulus ( $\mathcal{E} = \frac{3}{16} \sqrt{\frac{3K_{\text{wet}}\gamma}{\pi R_{\text{wet}}}}$ ), then

$$\sigma_{\text{Griffith}} \sim \sqrt{\frac{\gamma}{R_{\text{wet}}}} \sqrt{\frac{K_{\text{wet}}\gamma}{R_{\text{wet}}}} = \frac{\gamma^{3/4} K_{\text{wet}}^{1/4}}{R_{\text{wet}}^{3/4}}. \quad (3)$$

Comparing the ratio of the perfect-crystal and Griffith criterion,

$$\frac{\sigma}{\sigma_{\text{Griffith}}} \sim \left( \frac{\gamma}{K_{\text{wet}} R_{\text{wet}}} \right)^{1/4} = \mathcal{O}(1) \quad (4)$$

when we use physical quantities that describe our experimental system ( $R_{\text{wet}} = 67 \mu\text{m}$ ,  $K_{\text{wet}} = 22.5 \text{ kPa}$ , and  $\gamma = 72 \text{ mN m}^{-1}$ ). Thus,

$$\sigma_{\text{cap}} \sim \sigma_{\text{Griffith}}. \quad (5)$$

Therefore, while perfect-crystal behavior is not perfectly representative of our experiments, it is reasonable to approximate the experimental system as a perfect crystal by these scaling arguments. Nonetheless, our theory is compatible with the Griffith criterion.

## Supplementary Figures

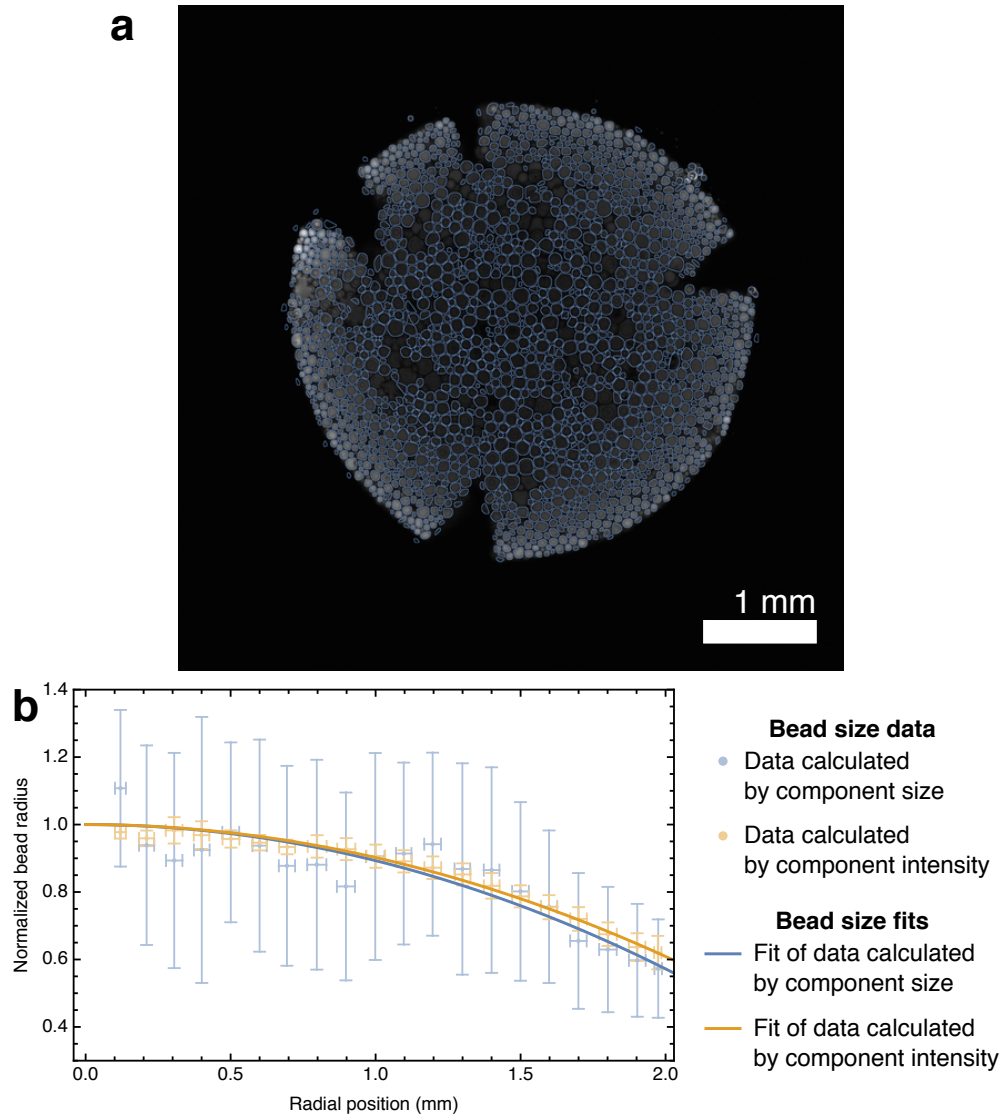


Figure S1: Measuring fluorescence intensity of beads is a viable and precise method of determining bead size. (a) We segmented a test image of reversible cracking into individual bead components. We then measured the bead size using two methods: by direct measurement of the size of the segmented components (blue) and by measurement of the fluorescence intensity of the segmented components (orange). (b) Plotting the normalized bead size—in reference to the largest bead size in the interior—as a function of radial position, we can see that there is little difference from the two methods. Both methods reveal a gradient in bead size to which we fit a parabolic curve for the purpose of comparison. The difference in these fits is at most 5%. The precision of the fluorescence-intensity method, however, is approximately an order of magnitude better than the direct-size method as indicated by the smaller error bars associated in the orange data points. Error bars correspond to one standard deviation of the scatter in the data.

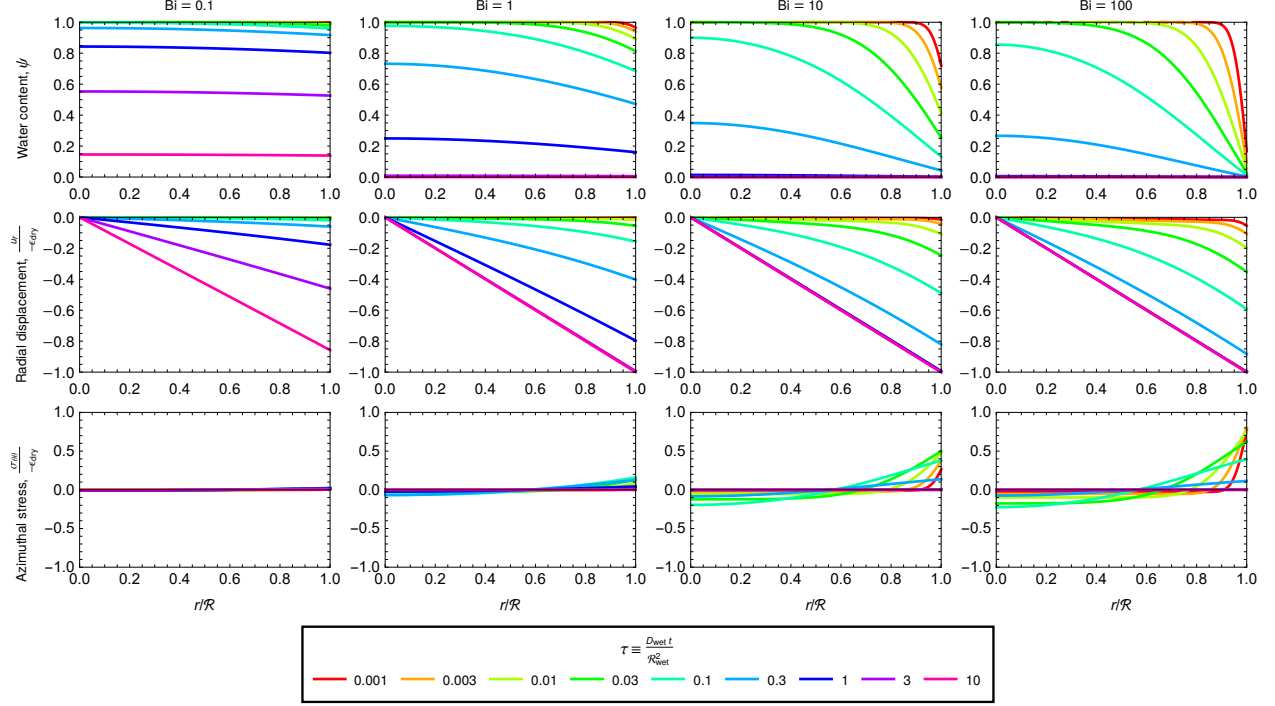


Figure S2: Nondimensionalized analytical solutions to the simplified continuum model demonstrate the influence of the Biot number. For each plot,  $r/\mathcal{R}$  on the abscissa and each curve represents the solution at a given nondimensional time—quantified by the Fourier number ( $\tau \equiv D_{wet} t / \mathcal{R}_{wet}^2$ ). (a) The water content solution (Eq. 4), as nondimensionally quantified by  $\psi$ , shows more differential shrinkage (more downward sloping curves) with increasing  $Bi$ . (b) The radial displacement (Eq. 9), as nondimensionally quantified by  $-u_r/\epsilon_{dry}$  ( $\epsilon_{dry} < 0$ ) also describes this differential shrinkage increase with  $Bi$ . This shrinkage increase is shown by the stronger downward concavity at higher  $Bi$ . Note that  $u_r < 0$  since the radial coordinate is directed outward and overall motion of the packing is inward. (c) The increased differential shrinkage with  $Bi$  also increases the azimuthal stress (Eq. 10), which is nondimensionally quantified by  $-\sigma_{\theta\theta}/\epsilon_{dry}$ . Positive values represent tension between beads while negative values represent compression. Stress with the highest magnitudes are tensile and occur at the periphery.

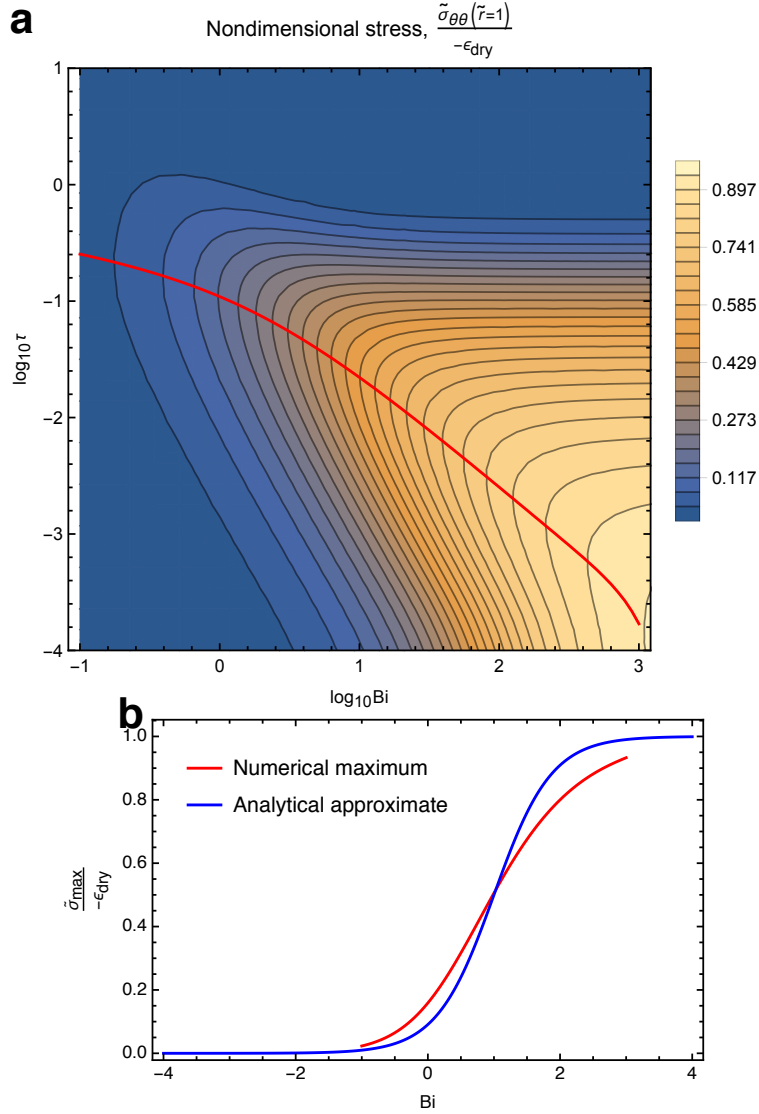


Figure S3: The maximum stress (red curves) in Biot–Fourier space (top) and as a function of Biot number (bottom). The top graph plots contours of  $-\sigma_{\theta\theta}/\epsilon_{\text{dry}}$  while the bottom plots  $-\sigma_{\theta\theta}/\epsilon_{\text{dry}}$  as a function of Biot number ( $\epsilon_{\text{dry}} < 0$ ). The red curve is the true numerical maximum stress at a given Biot number, which cannot be expressed in closed form, while the blue curve is an analytical approximation (Eq. 11) used in developing our cracking criteria.

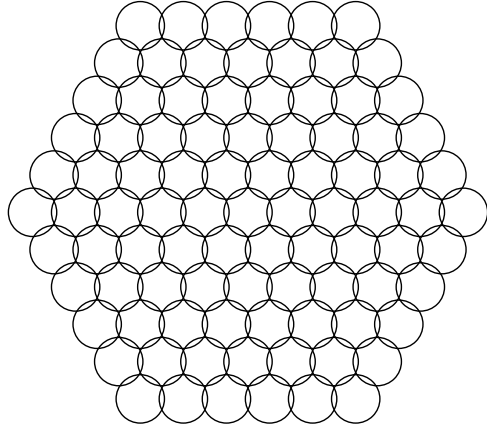


Figure S4: Ordered packing initial configuration (wet state). The bead radii are uniformly  $\hat{R}_{\text{wet}} = 1$ . Initial bonds are placed where beads overlap. The structure is perfectly hexagonal-close-packed.

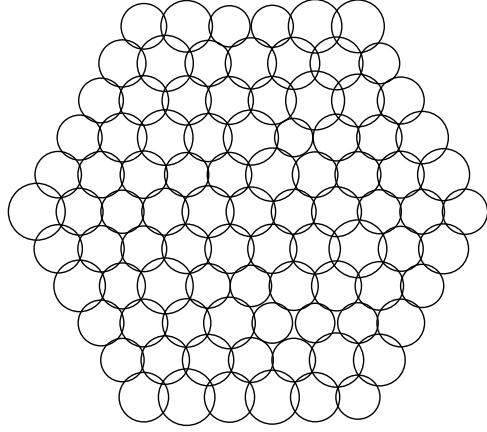


Figure S5: Disordered packing initial configuration. The bead radii are randomized according to a Gaussian distribution ( $\mu = \hat{R}_{\text{wet}} = 1$ ,  $\sigma = 0.1\hat{R}_{\text{wet}} = 0.1$ ). Initial bonds are placed where beads overlap. There are no bonds where beads do not overlap; thus, there are certain bonds missing when compared to the ordered case (Fig. S4).

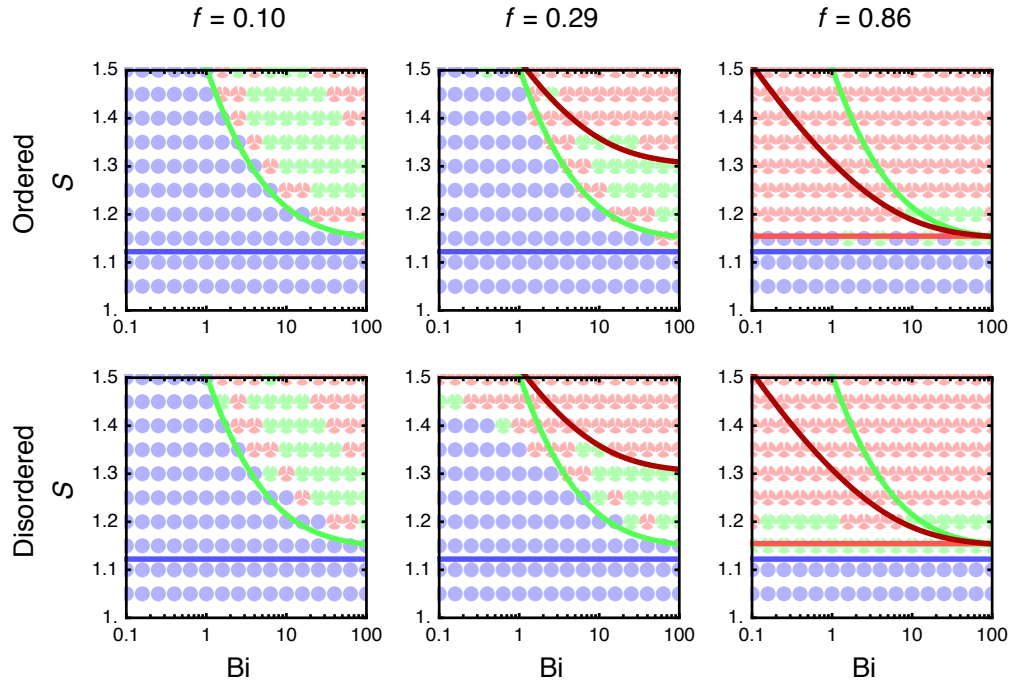


Figure S6: State diagrams of ordered (Fig. S4) and disordered (Fig. S5) systems where  $\hat{\delta}_{\text{wet}} = 0.22$  and  $M = 91$ .

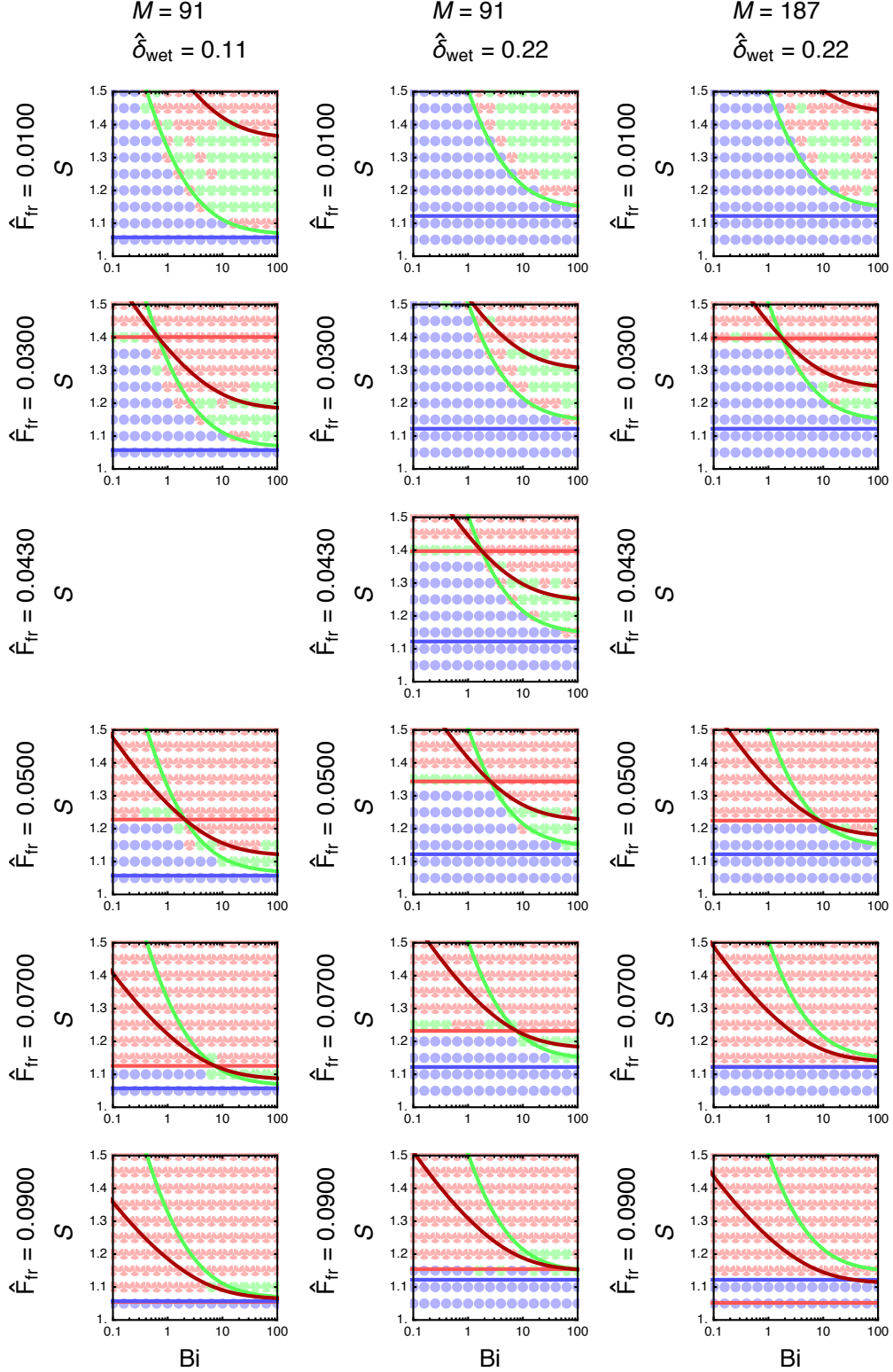


Figure S7: State diagrams of all DEM simulations performed and cracking criteria (Eqs. 13,14,15,16). Cracking behaviors were classified according to the number of bond breaks and the distances between beads at the dry state (see Materials and Methods). The occurrence of a small fraction of data points being inconsistent with cracking criteria, e.g. IC points in an RC region, can be attributed to an artifact of arbitrary classification rules.

## Supplementary Videos

### Supplementary Video S1

A small packing does not crack as it is dried (NC).

### Supplementary Video S2

A medium-sized packing cracks and self-closes (RC).

### Supplementary Video S3

A large packing irreversibly cracks into clusters (IC).

### Supplementary Video S4

Capillary bridges between hydrogel beads break as crack propagates.

### Supplementary Video S5

A DEM simulation of NC behavior.  $\hat{\delta}_{\text{wet}} = 0.22$ ,  $\hat{F}_{\text{fr}} = 0.01$ ,  $M = 187$ ,  $f = 0.14$ ,  $\text{Bi} = 0.10$ .

### Supplementary Video S6

A DEM simulation of RC behavior.  $\hat{\delta}_{\text{wet}} = 0.22$ ,  $\hat{F}_{\text{fr}} = 0.01$ ,  $M = 187$ ,  $f = 0.14$ ,  $\text{Bi} = 15.85$ .

### Supplementary Video S7

A DEM simulation of IC behavior.  $\hat{\delta}_{\text{wet}} = 0.22$ ,  $\hat{F}_{\text{fr}} = 0.03$ ,  $M = 187$ ,  $f = 0.41$ ,  $\text{Bi} = 15.85$ .